Title

Viral capsomere structure, surface processes and growth kinetics in the crystallization of macromolecular crystals visualized by in situ atomic force microscopy

Journal

Journal of Crystal Growth, 232(1-4)

ISSN

0022-0248

Authors

Malkin, AJ
Kuznetsov, Yu G
McPherson, A

Publication Date

2001-11-01

DOI

10.1016/s0022-0248(01)01063-6

ELSEVIER

Journal of Crystal Growth 232 (2001) 173–183

JOURNAL OF CRYSTAL GROWTH

www.elsevier.com/locate/jcrysgro

Viral capsomere structure, surface processes and growth kinetics in the crystallization of macromolecular crystals visualized by in situ atomic force microscopy

A.J. Malkin*, Yu.G. Kuznetsov, A. McPherson

Department of Molecular Biology and Biochemistry, University of California, Irvine, CA 92697, USA

Abstract

In situ atomic force microscopy (AFM) was used to investigate surface evolution during the growth of single crystals of turnip yellow mosaic virus (TYMV), cucumber mosaic virus (CMV) and glucose isomerase. Growth of these crystals proceeded by two-dimensional (2D) nucleation. For glucose isomerase, from supersaturation dependencies of tangential step rates and critical step length, the kinetic coefficients of the steps and the surface free energy of the step edge were calculated for different crystallographic directions. The molecular structure of the step edges, the adsorption of individual virus particles and their aggregates, and the initial stages of formation of 2D nuclei on the surfaces of TYMV and CMV crystals were recorded. The surfaces of individual TYMV virions within crystals were visualized, and hexameric and pentameric capsomers of the $T = 3$ capsids were clearly resolved. This, so far as we are aware, is the first direct visualization of the capsomere structure of a virus by AFM. In the course of recording the in situ development of the TYMV crystals, a profound restructuring of the surface arrangement was observed. This transformation was highly cooperative in nature, but the transitions were unambiguous and readily explicable in terms of an organized loss of classes of virus particles from specific lattice positions.

PACS: 81.10.Dn; 68.10.Jy; 68.35.Bs; 61.72. −y

Keywords: A1. Atomic force microscopy; A1. Biocrystallization; A1. Surface processes; A1. Surface structure

1. Introduction

Recent years have seen the convergence of a variety of technologies for the determination of the structural and even dynamic properties of supramolecular assemblies [1,2]. For example, cryo-electron microscopy is now used as a means of obtaining low-resolution phase information for complex assemblies such as large viruses [3], which is then extended to high resolution by X-ray diffraction. As we show here, atomic force microscopy (AFM) may also be a useful tool for obtaining similar information. Because it can be applied under essentially physiological conditions, in aqueous media, it may in many cases be superior to other microscopic techniques which

*Corresponding author. Tel.: +1-949-824-4397; fax: +1-949-824-1954.

E-mail address: amalkin@uci.edu (A.J. Malkin).

0022-0248/01/$ - see front matter
PII: S0022-0248(01)01063-6

require dehydration, freezing, or staining, or potentially otherwise perturb the structures of the samples.

The clarity with which structural detail can be seen on the surfaces of small viruses, here TYMV which has a diameter of only about 28 nm, suggests that AFM may be even more broadly useful as an analytical tool. Many viruses cannot be crystallized at all, or have unit cells beyond the range of X-ray crystallography. In those cases, as suggested here, AFM may provide an insightful approach to study, not only large virus structure, but also dynamic processes such as assembly and decapsidation [4,5].

In the past several years scanning tunneling microscopy (STM) has been successfully applied to studies of atomic mobility and surface evolution of crystalline materials grown in ultra high vacuum [6,7]. These results have been used in a number of practical applications, including development of electronic, optoelectronic and superconducting devices. In contrast, experimental data on molecular dynamics on surfaces of macromolecular crystals, a governing factor in the development of a quantitative understanding of the crystal growth process, are virtually absent.

Scanning probe microscopies, including AFM, have also had a major impact on the field of nanoscale materials science, where they have provided information about molecular interactions and conformation [8]. They have also served as mechanisms for molecular repositioning [9,10] and selective cleavage of molecular bonds [11]. They have been used to investigate reconstruction of semiconductor surfaces upon cleavage, epitaxial growth, annealing, deposition of surfactant layers, even controlled manipulation of individual atoms [12]. These kinds of investigations have not been widely applied in structural biology because of the fragile character of the materials and their liquid environments.

This study represents an initial attempt to study the structural features of macromolecules and their molecular dynamics on the surfaces of macromolecular crystals using a large particle amenable to both manipulation and detailed visualization. Because of icosahedral geometry, virions have virtually a spherical, completely uniform shape at the nanometer level. Sixtyfold symmetry provided by multiple identical protein subunits results in identical countenance from every direction. These properties along with large size of virions make icosahedral viruses virtually a perfect system to study surface phenomena and growth mechanisms at molecular resolution, where even events involving an individual virus particle can be recorded. Using in situ AFM we demonstrated that the growth of the (1 0 1) face of turnip yellow mosaic virus (TYMV) and the (1 1 0) face of cucumber mosaic virus (CMV) crystals proceeds strictly by two-dimensional nucleation. We have been able to image growth step edges as well as observe the adsorption of individual virus particles, their clusters, and record the initial stages of formation of 2D nuclei on crystalline surfaces. The capsomere structures of virions immobilized within crystals of TYMV were visualized along with cooperative restructuring of the TYMV crystal surface. We also describe here the results of studies of the surface morphology and kinetics of growth for glucose isomerase crystals.

2. Experimental section

Turnip yellow mosaic virus (TYMV), a $T = 3$ icosahedral plant virus of 28 nm diameter, is one of the most thoroughly studied of all viruses [13–17]. The TYMV genome is made up of $M_r = 1.9 \times 10^6$ single-stranded RNA of 6218 bases [16], and a 694 nucleotide subgenomic RNA that is included in most virions. The structure of the virus was determined by X-ray diffraction analysis [18,19] from bipyramidal crystals (space group $P6_422$ with $a = b = 515.0$ Å and $c = 309.4$ Å) grown from virus purified from Chinese cabbage by conventional procedures [13,18]. The capsid of TYMV is composed of 180 identical protein subunits, each of about 20 kDa, organized into 12 pentameric and 20 hexameric capsomers which project about 40 Å above the surface of the virion [17,19]. TYMV crystals were grown by the vapor diffusion method [20] consisting of mixing 10–16 mg/ml TYMV in H_2O with 0.8–1.0 M ammonium phosphate in 100 mM MES at pH. 3.5 and equilibrating

droplets of this mother liquor against reservoirs of 1.0 M ammonium phosphate.

Crystals of cucumber mosaic virus (CMV), a $T = 3$ icosahedral plant virus of 28 nm diameter ($M_r = 5.5 \times 10^6$) were grown by mixing 3–5 mg/ml CMV in water with 22–25% saturated ammonium sulfate, 50 mM MES, pH 6.5 and equilibrating droplets of this mother liquor against reservoirs of 25% saturated ammonium sulfate. CMV crystals studied here diffract X-rays to only 5–6 Å resolution [21] and belong to the cubic space group I23 with the unit cell parameter $a = 336.0$ Å [21].

Glucose Isomerase ($M_r = 173\,000$) from *Streptomyces rubiginosus* was purchased from Hampton Research (Laguna Niguel, CA). The high-resolution structure of the orthorhombic crystals studied here (I222, $a = 94.01$ Å, $b = 99.37$ Å, $c = 103.01$ Å) has been determined [22]. Crystals of glucose isomerase were grown by the vapor diffusion method consisting of mixing 20–25 mg/ml of glucose isomerase in water with an equal amount of reservoir solution which consisted of 20% PEG400, 0.1 M Na Hepes, pH 7.5, 0.2 M magnesium chloride (Hampton Research Crystal Screen I).

Seed crystals for AFM experiments were nucleated and grown on glass substrates in a 10 μl droplet by vapor diffusion or a batch method. Crystals were then transferred into the AFM fluid cell, which was subsequently filled with a mixture of virus, or protein, and precipitant solution. Images were collected in tapping mode using a Nanoscope III AFM (Digital Instruments, Santa Barbara, CA) with Digital Instruments' oxide sharpened silicon nitride tips. Because of the exceptionally fragile character of the TYMV and CMV crystals application of the tapping mode method is essential. We were not successful in imaging TYMV and CMV crystals using contact mode. All operations were carried out under crystallization conditions, in a fluid filled cell, with supersaturation controlled by the concentration of precipitant, or by the virus or protein concentration. For glucose isomerase the reverse movement of growth steps for both growth and dissolution was observed. This allowed us to estimate an equilibrium concentration c_e as the midpoint at which crystals neither grew nor dissolved. Solution supersaturation σ was defined as $\ln(c/c_e)$ and $(c - c_e)$ where c and c_e are the initial and equilibrium protein concentration.

3. Results and discussion

3.1. Surface morphology of TYMV and CMV crystals

Growth of the (1 0 1) faces of TYMV crystals and (1 1 0) faces of CMV crystals occurred exclusively through two-dimensional nucleation and layer-by-layer step advancement (Fig. 1). No dislocation sources were observed. Typically, high densities of growth steps were consistently observed on surfaces of TYMV and CMV crystals. In the case of TYMV crystals, two-dimensional islands exhibited triangular shapes, as seen in Fig. 1(a), which indicates kinetic anisotropy in step advancement along different crystallographic directions. The heights of growth steps were 29 ± 2 nm and 25 ± 2 nm for TYMV and CMV crystals, respectively. These correspond well with the (1 0 1) and (1 1 0) interplanar distances deduced by X-ray diffraction [19,21].

Step advancement on the surfaces of growing TYMV and CMV crystals proceeds through one-dimensional nucleation [23] at the edges, which results in kink formation and, subsequently, their lateral advancement (Figs. 2a, 3a–c). A similar mechanism was recently observed for the step advancement on growing thaumatin and lysozyme crystals [24–28].

Because of the large size of virions, not only were the structures of step edges and their movements visible, but attachment of individual virus particles to the step edge, and adsorption of virions and their aggregates to crystalline surfaces, could be observed as well. In Figs. 2(a) and 3(a)–(c), for example, single kinks formed by individual virions or several virus particles can be seen. In Figs. 3(a)–(b) a two-dimensional nucleus on the surface of CMV crystal, formed by eleven virus particles, expanded by the addition of five new virus particles. Under the same conditions a number of individual virus particles (Figs. 2 and 3) and their clusters were also seen adsorbed to the

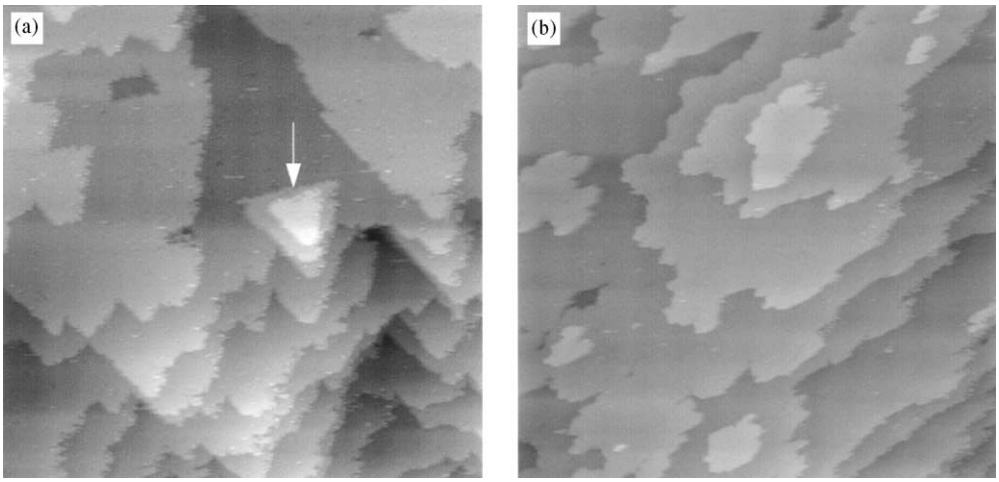

Fig. 1. Surface morphology of the (1 0 1) face of TYMV (a) and (1 1 0) face of CMV (b) crystals. In (a) two-dimensional islands having triangular shapes are indicated with an arrow. The scan areas are (a) $4 \times 4\,\mu m^2$; (b) $9.6 \times 9.6\,\mu m^2$.

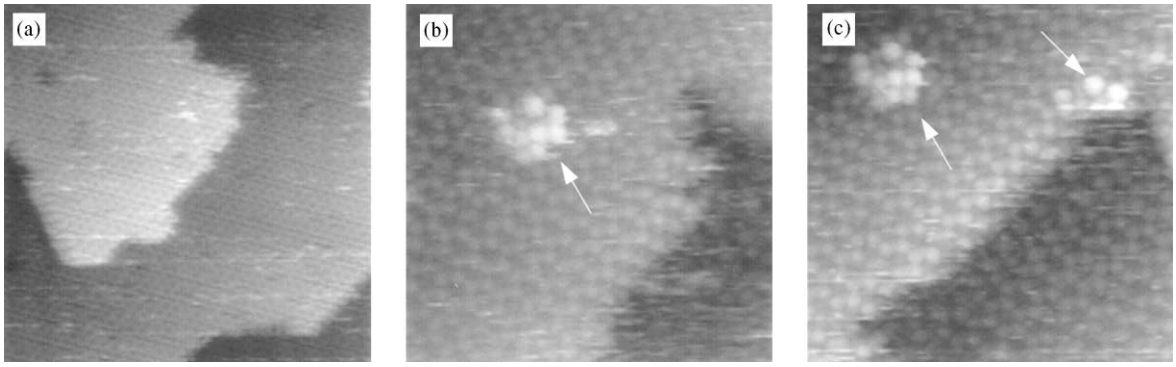

Fig. 2. In (a) structure of the growth step edge on a TYMV crystal surface. (b) Cluster of nine virus particles (indicated with an arrow) adsorbed on the crystalline surface. In (c) a new virus particle (indicated with an arrow) incorporated into the cluster as well as several other virus particles (indicated with an arrow). The scan sizes are (a) $2.25 \times 2.25\,\mu m^2$; (b) and (c) $800 \times 800\,nm^2$.

crystalline surface where they remained for an extended period of time. Fig. 2(b) contains a cluster of nine virus particles on the surface of a TYMV crystal. Over several scans the size of this cluster remained unchanged. After 10 min of observation, (Fig. 2(c)) addition of a single new particle to the cluster was recorded as well as adsorption of several other individual virus particles to the surface. Although these virus particles and aggregates are firmly attached to the crystalline surface, they do not develop into two-dimensional nuclei. This suggests that their interactions with the underlying surface are probably non-crystallographic. This could be caused, for example, by some minor modifications of their protein subunits or by contamination with some other $T = 3$ virus as well. These particles ultimately become incorporated into the growth steps. Considerably higher densities of these kinds of virions are seen on surfaces of CMV crystals compared with TYMV and STMV crystals. This could conceivably be the cause of the very poor diffraction properties of CMV crystals.

Detailed studies of molecular dynamics on the surfaces of TYMV and CMV crystals as a function of supersaturation, as well as underlying

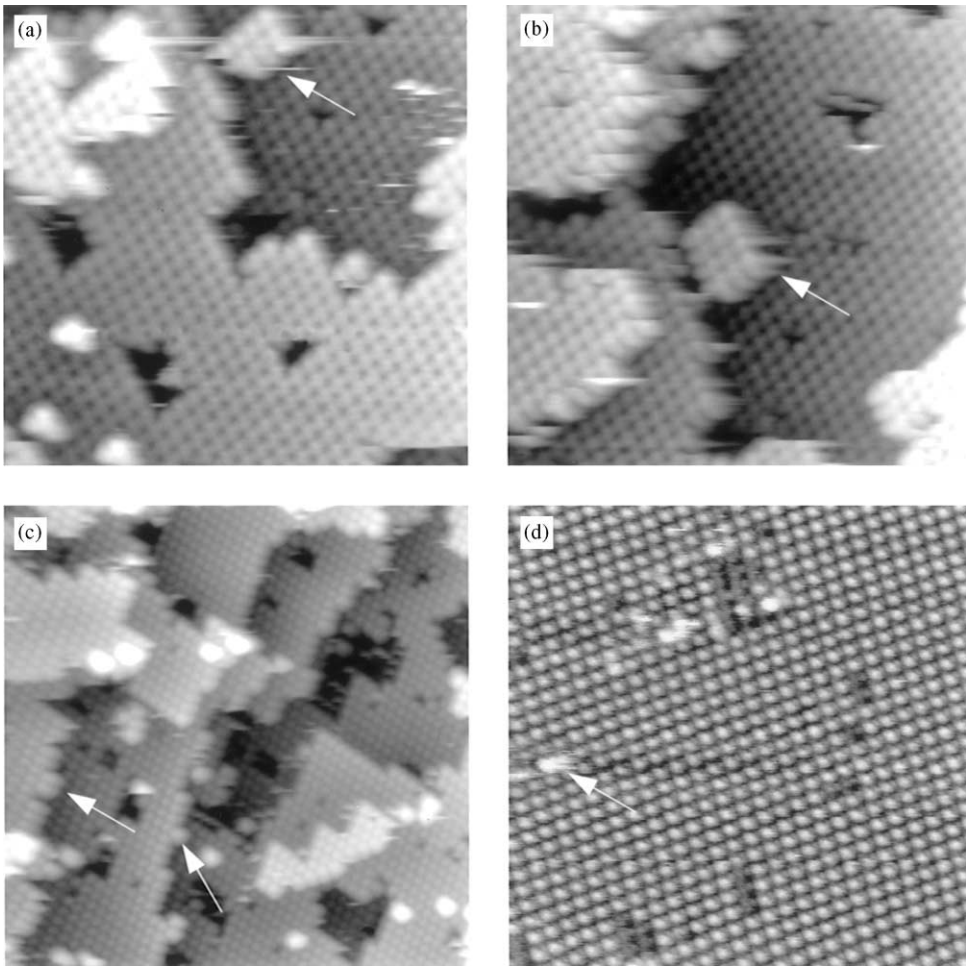

Fig. 3. In (a) and (b) growth of two-dimensional island (indicated with an arrow) on a CMV crystal surface. In (a) three adsorbed virus particles are seen in the left bottom part of the image. In (c) step kinks formed by single virion and two virus particles are indicated with an arrow. A number of adsorbed virions on the crystalline surface are seen as well as in (d). In (d) several vacancies are observed. The scan sizes are (a); (b) $860 \times 860\,nm^2$ and (c) $1.4 \times 1.4\,\mu m^2$ and (d) $750 \times 750\,nm^2$.

mechanisms of step motion are currently under investigation and will be presented elsewhere.

3.2. High resolution imaging of TYMV and CMV crystals

Figs. 4(a) and (b) present AFM images of individual virus particles making up the (1 0 1) plane of the TYMV crystals. Apparent in the images are broad, solvent filled channels that permeate the crystals and which have diameters roughly equivalent to that of a virion. The noteworthy features of the particles, which in this view are in the canonical orientation of the virion seen in Fig. 4(c), are the capsomers. Twelve capsomers are composed of five, and 20 capsomers of six protein subunits. Based on the known structure of TYMV and its arrangement in the crystals from X-ray diffraction data, as well as the 20% difference in their sizes, the pentameric and hexameric clusters can be discriminated in Fig. 4 from one another. Note that the difference between the highest and lowest points on the capsid surface, about 40 Å [19] is accurately

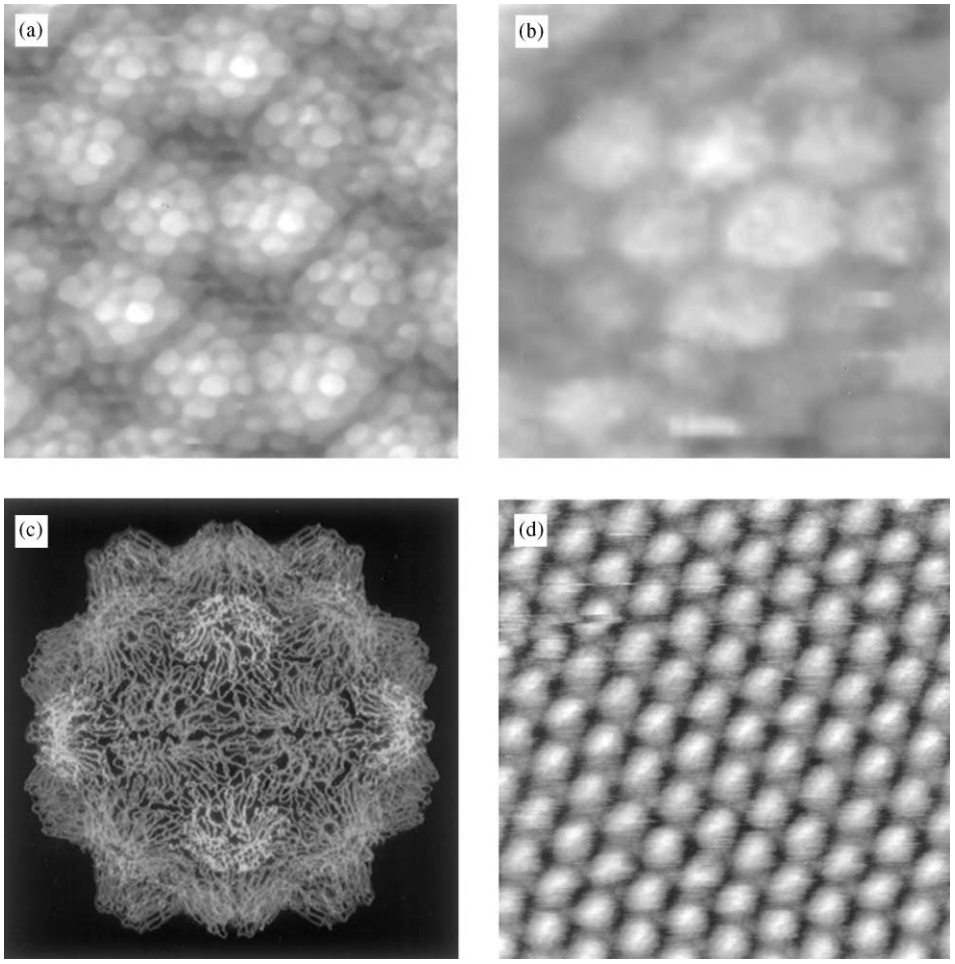

Fig. 4. In (a) and (b) in situ AFM images of TYMV particles immobilized in the crystalline lattice clearly display capsomers on the surface of the $T = 3$ icosahedral virions. The capsomers, from both X-ray diffraction [19] and AFM, are roughly 60 Å across and protrude above the viral surface by about 45 Å. (c) the structure of the capsid of TYMV based on X-ray diffraction analysis [19]. (d) Surface layer of (1 0 0) face of CMV crystal. The scan areas are (a) 140×140, (b) 38×38 and (c) $300 \times 300\,\text{nm}^2$.

reflected by AFM. The same measure for CMV of approximately 28 Å is smaller than that for TYMV. Although the height of capsomers in the case of CMV appears to be sufficient for visualization, we have not yet been able to resolve the capsomere structure of CMV (Fig. 4(c)). Studies of CMV crystallization are currently in their initial stages.

The images of single virus particles provided by AFM, the accurate depiction of their structural characteristics, as well as their exact positions and orientations in the crystal lattice, may prove useful for deducing initial phase information for X-ray diffraction. Initial phase information in virus crystallography is of particular value because structure determination relies only on extension of initial phases to high resolution using the icosahedral symmetry of the particles. The success of that process is directly dependent on the quality of the starting model used to formulate the initial phase set. The fact that capsomere structure is

clear even on such relatively small viruses as TYMV, is a propitious sign for the application of AFM to even larger, more complex samples.

3.3. Surface restructuring in TYMV crystallization

Larger scan areas of the surface layers of the (1 0 1) planes of the crystals revealed three distinctive arrangements of viral particles on the surfaces and these are presented in Fig. 5. When the supersaturation was reduced to equilibrium, it was observed on a number of TYMV crystals that the patterns transformed in time from one to another. Transitions occurred rapidly, as one motif was seen at the end of a scan and another motif at the beginning of the next, where a scan period was about 4–6 min. At these supersaturation conditions no two-dimensional nucleation was observed and the step growth rate was relatively low. There were no steps sweeping across the surface areas under observation during these transitions.

A defined area on the crystal surface yields a consistent, stable pattern over many consecutive scans before the restructuring occurs, hence we believe that the tip does not displace individual, weakly bound particles from the lattice. We cannot, however, rule out tip influence as a possible factor in promoting the transitions. AFM tip pressure could alter the chemical potential of lattice units, thereby causing particle release from the surface near equilibrium conditions. For other macromolecular crystals we have studied, more than a dozen [26,29–31], as well as for CMV crystals at equilibrium conditions, excessive tip pressure produced visible scarring of the crystalline surface, but not an organized, cooperative restructuring as we observe here.

The pattern seen in Fig. 5(a) was initially observed on the (1 0 1) surface layer. Transformation then occurred to yield that seen in Fig. 5(b), which subsequently restructured to yield the pattern seen in Fig. 5(c). The relationship between the three motifs, and the mechanism of transformation from one to another, is shown in Fig. 6. Starting with the motif in Fig. 5(a), and corresponding Fig. 6(a), removal of all particles of class A, which occupy specific locations in the crystallographic unit cells, yields the motif of Fig. 5(b), and corresponding Fig. 6(b). Further removal of all particles of class B, as seen in Fig. 6(b), produces the motif appearing in Fig. 5(c), and in corresponding Fig. 6(c). The process of surface restructuring was not reversible and the structure presented in Fig. 5(c) was stable for prolonged periods over the course of experiments, which typically lasted for 6–8 h. Note that hexagons, which can be clearly seen in Fig. 5(c), are formed by virions in positions $CA_1CA_1CA_1$ (Fig. 6(c)). Although there is some height difference between virions in positions C and A_1 (Fig. 6c, bottom), it is not apparent in experimental images (Fig. 5(c)).

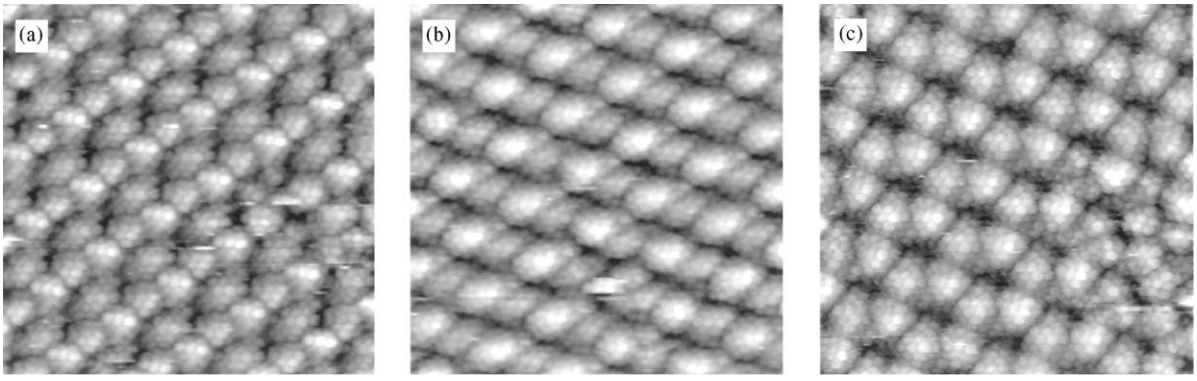

Fig. 5. (a)–(c) In situ, $300 \times 300\,nm^2$ AFM images recording sequential transformations of the surface layer of the (1 0 1) face of the TYMV crystals, when exposed to equilibrium conditions. Vacancies in the surface layer, where one or more individual particles are absent, were occasionally observed.

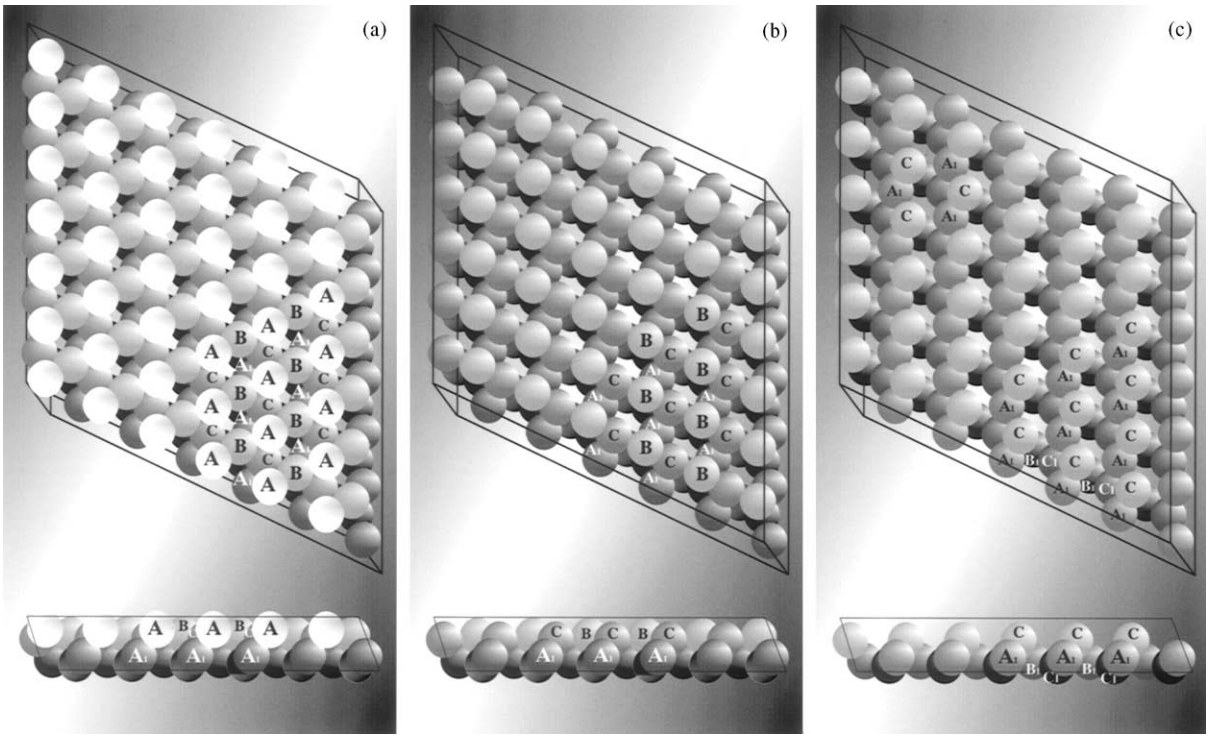

Fig. 6. Computer simulated orthogonal images of the different surface structures of the (1 0 1) faces of the TYMV crystals based on the packing of the particle known from X-ray diffraction. Each class of particles A–C correspond to viruses occupying symmetry related positions in the unit cell. Although these units are identical in the interior of the crystal, they are unique when in a surface layer. Sequential loss of particle class A from the motif in (a), corresponding to Fig. 5(a), yields the motif in (b), corresponding to Fig. 5(b). Subsequent loss of particle class B in (b) yields the motif in (c), which corresponds to that observed in Fig. 5(c). In (c) particles in positions C and A_1 (from the next layer down) form the hexagonal rings of particles seen in Figs. 4(a) and (b).

The same is true for virions in positions A and C in Fig. 5(c). This is because tapping mode AFM frequently does not produce entirely accurate height information compared with contact mode. Thus, the transformations can be described as an organized emission from the lattice of distinct classes of virus particles occupying specific crystallographic lattice positions. In each transition, the class of particles lost is that which protrudes highest above the surface, and which maintains least contact with the viruses forming the remainder of the crystal lattice. That is, the class which is least firmly bound and has the highest chemical potential.

The salient feature of the surface transitions observed here by AFM is their organized, cooperative nature. Unlike normal dissolution, as seen particularly in etching experiments [32,33], the release of molecules from the crystals does not occur in a sequential manner, molecule after molecule, at step edges or at sensitive points of high chemical potential such as defects. Currently, we are initiating additional studies on the influence of supersaturation and temperature on surface transitions in TYMV crystallization.

3.4. Surface morphology and growth step kinetics of glucose isomerase crystals

Growth steps on the (0 0 1) face of orthorhombic glucose isomerase crystals were generated by two-dimensional nuclei (Fig. 7). The step height of 100 ± 3 Å is equal to the unit cell parameter along *c*. It may be noteworthy that the concentration of

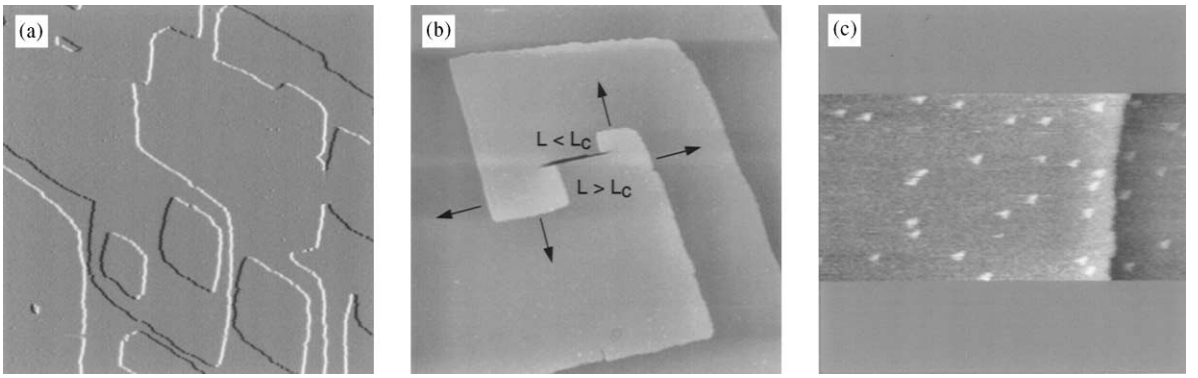

Fig. 7. (a) $11 \times 11\,\mu m^2$ image showing 2D nucleation on the surface of glucose isomerase crystal. (b) $11 \times 11\,\mu m^2$ image showing growth steps advancing around the stacking fault. Arrows indicate advancing steps segments. (c) $5.5 \times 11\,\mu m^2$ image showing adsorbed impurities on the surface of glucose isomerase crystal.

PEG affects the rate of 2D nucleation independent of supersaturation. For example 2D nucleation takes place at relatively low supersaturations, $\sigma < 1$, when PEG concentration of 3% and higher is utilized. At lower concentrations of PEG, 2D nucleation was virtually absent even at the highest protein concentrations we investigated. There was no 2D nucleation even when high concentrations of protein were utilized along with 2% PEG so that the resulting supersaturation was $\sigma > 2$. Based on this observation one possibility is that PEG molecules could adsorb on the crystalline surface and serve as a source of heterogeneous nucleation, however, a more comprehensive understanding of this phenomena requires additional experiments.

In one experiment we observed on a crystal surface the combination of a stacking fault with dislocation sources, which resulted in rotation of two growth steps around the stacking fault (Fig. 7(b)). We measured the supersaturation dependencies of tangential step rates for four orthogonal crystallographic directions (Fig. 8) using the stacking fault as a reference point.

The tangential step rate, v is given by [34]

$$v = \Omega\beta(c - c_e), \tag{1}$$

where $\Omega = 4.8 \times 10^{-19}$ is the specific volume of a glucose isomerase tetramer in the crystal, c and $c_e = 2.1 \times 10^{15}\,cm^{-3}$ are initial and equilibrium concentrations of protein, respectively, and β is the step kinetic coefficient [35]. From the linear

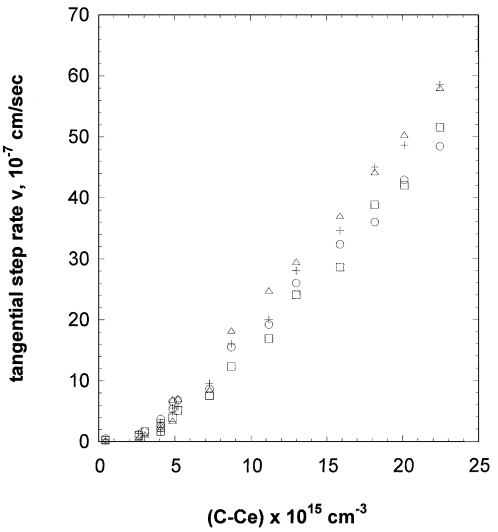

Fig. 8. Supersaturation dependencies of tangential step growth rates in different crystallographic directions. $\langle 0\,1\,0\rangle$ (squares); $\langle 1\,0\,0\rangle$ (triangles); $\langle \bar{1}\,0\,0\rangle$ (crosses) and $\langle 0\,\bar{1}\,0\rangle$ (circles).

portion of $v(c - c_e)$ dependencies for $(c - c_e) > 10^{14}\,cm^{-3}$ (Fig. 8), the kinetic coefficient β for glucose isomerase crystallization was estimated to be 4.7×10^{-4}, 5.2×10^{-4}, 4.4×10^{-4} and 5.4×10^{-4} cm/s for crystallographic directions $\langle 0\,1\,0\rangle$, $\langle \bar{1}\,0\,0\rangle$, $\langle 0\,\bar{1}\,0\rangle$, $\langle 0\,\bar{1}\,0\rangle$ and $\langle 1\,0\,0\rangle$, respectively. Similar values for the kinetic coefficient were found for the crystallization of several other macromolecules [31,36–38]. The lower values of β for macromolecular crystallization compared

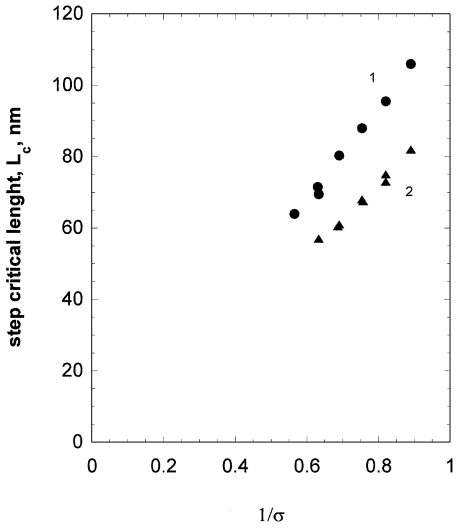

Fig. 9. Dependence of step critical length on supersaturation for 1, $\langle 0\,\bar{1}\,0\rangle$; 2, $\langle 1\,0\,0\rangle$.

with inorganic crystallization [35] has been attributed to the necessity of the pre-kink selection of the proper orientation of an incoming macromolecule for incorporation into the growth step [28]. At lower supersaturation a non-linear dependency of tangential step rate was observed (Fig. 8), presumably due to the influence of impurities, a phenomenon well documented for a number of other macromolecular and inorganic crystals [38]. Longer storage of protein solution resulted in increased amounts of impurities, presumably due to the aggregation or degradation of glucose isomerase. We were able to see adsorption of impurities on the surface and their incorporation into the steps (Fig. 7(c)).

Growth steps advance (Fig. 7(b)) only when their length L exceeds a critical value, L_c, [35]. Critical length L_c is related to the free energy of the step edge α by [35]

$$L_c = 2\Omega\alpha/kT\sigma, \tag{2}$$

where k is the Boltzmann's constant and T the temperature. Supersaturation dependence of step critical length, L_c, was measured as the average of growth step length immediately before and after the growth step started to advance (Fig. 9). From the slope of L_c $(1/\sigma)$ dependencies, according to Eq. (2), surface free energies of the step edge α were estimated to be 0.5 and 0.37 erg/cm^2 for $\langle 0\,\bar{1}\,0\rangle$ and $\langle 1\,0\,0\rangle$ crystallographic directions, respectively.

4. Conclusions

The results presented here show that, using tapping mode AFM, the capsomere structures of viruses can be reliably visualized and, to at least some extent, characterized. The correlation with X-ray diffraction at the same resolution is excellent. Because of the large size of the lattice unit, an entire virion, the crystals possess a number of unique properties when compared with conventional crystals, and even with other macromolecular crystals. Furthermore, the large particle size allows studies of dynamic processes on the crystalline surface, opportunities not otherwise available. The surface restructuring presented here represents the first example of such a mass cooperative process that we have observed for any macromolecular crystals under study. The surface morphology and growth kinetics for glucose isomerase crystals was studied over wide supersaturation range. From the supersaturation dependencies of tangential step rates and step critical length, the kinetic coefficient of steps β and the surface free energy α were calculated.

Acknowledgements

This research was supported by National Aeronautics and Space Administration. We would like to thank R. Lucas and J. Day for TYMV and CMV purification, J. Zhou for screening crystallization conditions for glucose isomerase and A. Greenwood for assistance in preparation of figures.

References

[1] J. King, W. Chiu, in: W. Chiu, R.M. Burnett, R. Garcea (Eds.), Structural Biology of Viruses, Oxford University Press, Oxford, 1997, p. 288.

[2] A.C. Steven, P.G. Spear, in: W. Chiu, R.M. Burnett, R. Garcea (Eds.), Structural Biology of Viruses, Oxford University Press, Oxford, 1997, p. 312.
[3] T.S. Baker, J.E. Johnson, in: W. Chiu, R.M. Burnett, R. Garcea (Eds.), Structural Biology of Viruses, Oxford University Press, Oxford, 1997, p. 38.
[4] S. Casjens, Virus Structure and Assembly, Jones and Barlett Inc., Boston, 1985.
[5] J.M. Kaper, The Chemical Basis of Virus Structure, Dissociation and Reassembly, North-Holland, Amsterdam, 1975.
[6] M.G. Lagally, Phys. Today 46 (1993) 24.
[7] Z.Y. Zhang, M.G. Lagally, Science 276 (1997) 377.
[8] T.A. Jung, R.R. Schlitter, J.K. Gimzewski, Nature 386 (1997) 696.
[9] T.A. Jung, R.R. Schlitter, J.K. Gimzewski, H. Tang, C. Joachim, Science 271 (1996) 181.
[10] G. Meyer, L. Bartels, S. Zophel, E. Henze, K.-H. Reider, Phys. Rev. Lett. 78 (1997) 1512.
[11] J.K. Gimzewski, T.A. Jung, M.T. Cuberes, Schlittler, Surf. Science 386 (1997) 101.
[12] G.P. Srivastava, Rep. Progr. Phys. 60 (1997) 561.
[13] R. Markham, K.M. Smith, Parasitology 39 (1949) 330.
[14] R.E.F. Matthews, Plant Virology, third Edition, Academic Press, San Diego, 1991.
[15] J.T. Finch, A. Klug, J. Mol. Biol. 15 (1966) 344.
[16] L. Hirth, L. Givord, in: R. Koenig (Ed.), The Plant Viruses, Vol. 3, Plenum, New York, 1988, p. 163.
[17] J.E. Mellema, L.A. Amos, J. Mol. Biol. 72 (1972) 819.
[18] M.A. Canady, J. Day, A. McPherson, Proteins 21 (1995) 78.
[19] M.A. Canady, S.B. Larson, J. Day, A. McPherson, Nat. Struct. Biol. 3 (1996) 771.
[20] A. McPherson, Crystallization of Biological Macromolecules, Cold Spring Harbor Laboratory Press, Cold Spring Harbor, 1998.
[21] W.W. Wikoff, C.J. Tsai, G. Wang, T.S. Baker, J.E. Johnson, Virology 232 (1997) 91.
[22] Z. Dauter, H. Witzel, K.S. Wilson, Acta Crystallogr, Sect. B 46 (1990) 833.
[23] V.V. Voronkov, Sov. Phys. Crystallogr. 15 (1970) 13.
[24] A.A. Chernov, Acta Crystallogr. A 54 (1998) 859.
[25] L.N. Rashkovich, N.V. Gvozdev, I.V. Yaminsky, Cryst. Rep. 43 (1998) 696.
[26] Yu.G. Kuznetsov, A.J. Malkin, A. McPherson, J. Crystal Growth 196 (1999) 489.
[27] Yu.G. Kuznetsov, J. Konnert, A.J. Malkin, A. McPherson, Surf. Science 440 (1999b) 69.
[28] A.A. Chernov, L.N. Rashkovich, I.V. Yaminsky, N.V. Gvozdev, J. Phys.: Condens. Matter 11 (1999) 9969.
[29] A.J. Malkin, Yu.G. Kuznetsov, T.A. Land, J.J. DeYoreo, A. McPherson, Nature Struct. Biol. 2 (1995) 956.
[30] A.J. Malkin, T.A. Land, Yu.G. Kuznetsov, J.J. DeYoreo, A. McPherson, Phys. Rev. Lett. 75 (1995) 2778.
[31] A.J. Malkin, Yu.G. Kuznetsov, W. Glantz, A. McPherson, J. Phys. Chem. 100 (1996) 11736.
[32] A.J. Malkin, Yu.G. Kuznetsov, A. McPherson, Surf. Sci. 393 (1997) 95.
[33] A.J. Malkin, Y.G. Kuznetsov, A. McPherson J. Struct. Biol. 117 (1996) 124.
[34] A.A. Chernov, in: M. Cardona, P. Fulde, H.-J. Queisser (Eds.), Modern Crystallography III. Crystal Growth, Vol. 36, Springer, Berlin and New York, 1984, p. 249.
[35] A.A. Chernov, H. Komatsu, in: J.P. van der Eerden, O.S.L. Bruinsma (Eds.), Science and Technology of Crystal Growth, Kluwer Academic, Netherlands, 1995, p. 67.
[36] T.A. Land, J.J. DeYoreo, J.D. Lee, Surf. Sci. 384 (1997) 136.
[37] P.G. Vekilov, F. Rosenberger, J. Crystal Growth 158 (1996) 540.
[38] A.J. Malkin, Yu.G. Kuznetsov, A. McPherson, J. Crystal Growth (1999) 471.